Multidimensional solitons in a low-dimensional periodic potential

Bakhtiyor B. Baizakov,[1] Boris A. Malomed,[2] and Mario Salerno[1]
[1]*Dipartimento di Fisica "E.R. Caianiello" and Istituto Nazionale di Fisica della Materia (INFM), Università di Salerno, I-84081 Baronissi (SA), Italy*
[2]*Department of Interdisciplinary Studies, Faculty of Engineering, Tel Aviv University, Tel Aviv 69978, Israel*
(Received 21 June 2003; revised manuscript received 4 May 2004; published 18 November 2004)

Using the variational approximation and direct simulations in real and imaginary time, we find stable two-dimensional (2D) and 3D solitons in the self-attractive Gross-Pitaevskii equation (GPE) with a potential which is uniform in one direction (z) and periodic in the others (however, the quasi-1D potentials cannot stabilize 3D solitons). The family of solitons includes single- and multiple-peaked ones. The results apply to Bose-Einstein condensates (BEC's) in optical lattices (OL's) and to spatial or spatiotemporal solitons in layered optical media. This is the first prediction of *mobile* 2D and 3D solitons in BEC's, as they keep mobility along z. Head-on collisions of in-phase solitons lead to their fusion into a collapsing pulse. Slow collisions between two multiple-peaked solitons whose main peaks are separated by an intermediate channel end up with their fusion into one single-peaked soliton in the middle channel, $\simeq 1/3$ of the original number of atoms being shed off. Stable localized states in the self-repulsive GPE with the low-dimensional OL combined with a parabolic trap are found too. Two such pulses in one channel perform recurrent elastic collisions, periodically featuring sharp interference patterns in the strong-overlap state.

DOI: 10.1103/PhysRevA.70.053613 PACS number(s): 03.75.Kk, 05.45.−a, 05.30.Jp

I. INTRODUCTION

Solitons in multidimensional (multi-D) nonlinear Schrödinger equations (NLSE's) with a periodic potential have recently attracted considerable interest. In particular, self-trapping of spatial beams in nonlinear photonic crystals is described by a 2D equation. In this case, simulations reveal robust 2D solitons in the self-focusing model [1]. A similar medium can be created by a grid of laser beams illuminating a photorefractive sample [2].

Similar 2D and 3D models with a periodic potential describe a Bose-Einstein condensate (BEC) trapped in an optical lattice (OL). This realization is especially important, as experimental techniques for loading BEC's into multi-D OL's were recently developed [3]. Stable solitons can be supported by an OL even in self-repulsive BEC's [4–6]. In the case of self-attraction, 2D and 3D solitons (including 2D vortices) are stable in the self-focusing model with the OL potential [7], despite the possibility of the collapse [8].

An issue of direct physical relevance, which is the subject of the present work, are multi-D solitons in media with periodic potentials of a *lower dimension* (low D)—viz., quasi-1D (Q1D) and Q2D lattices in the 2D and 3D cases, respectively. In optics, the 2D equation in the spatial domain governs the beam propagation in a layered bulk medium along the layers, which extends a 1D multichannel system introduced in Ref. [9], with the potential induced by transverse modulation of the refractive index (RI). For a typical case with the periodicity of the transverse modulation ~ 30 μm, the diffraction length of the corresponding spatial soliton is ~ 1 cm. In the temporal domain, the 2D and 3D equations govern, respectively, the longitudinal propagation of spatiotemporal optical solitons in a layered planar waveguide or in a bulk medium with the RI periodically modulated in both transverse directions. The 2D and 3D cases directly apply to BEC's loaded in a Q1D or Q2D lattice, this realization being much closer (than in optics) to the real experiment in the 3D case. In that case, the characteristic OL periodicity ~ 0.5 μm implies the soliton's formation time ~ 1 ms, in the OL with the strength ~ 10 recoil energies.

The physical significance of these settings is twofold: first, in the experiment it is much easier to create low-D lattices than full-dimensional ones, both in BEC's and in optics; hence, they offer the most straightforward way to create multi-D solitons. Second, the solitons created this way can freely move in the unconfined direction, which suggests a possibility to study their collisions and to look for their bound states. As yet, no other way to create multi-D *mobile* solitons in BEC's and their bound states, thus making it possible to manipulate the matter-wave pulses, has been proposed. Below, we demonstrate that nontrivial interactions between colliding solitons (matter exchange, collapse, interference effects, etc.) occur, in BEC's with the above-mentioned values of the physical parameters, in the range of velocities ~ 1 mm/s. This range can be readily altered by changing the OL strength.

It is appropriate to mention essential differences of multi-D solitons in a periodic potential from counterparts in the axially symmetric 3D Gross-Pitaevskii equation (GPE) [10,11]. Primarily, it concerns the following spatial features: multi-D soliton in a periodic potential can have a multihump structure, extending itself over several lattice cites [see Figs. 3(b) and 5]. Second, multi-D solitons in a low-D periodic potential can experience off-center collisions [see Figs. 8, 10, and 11], which is impossible with solitons in the axially symmetric 3D models. It is the transverse degree of freedom which attributes multi-D solitons in a periodic potential truly 3D features. With regard to similarities, one can mention the inelasticity of collisions of multi-D solitons in both models. Again, off-center collisions of multi-D solitons moving in adjasent tracks of the OL can reveal new types of inelastic interactions—e.g., merging of two solitons in the intermedi-

ate channel by shedding off the excessive mass (see Fig. 11). Another common feature of multi-D solitons in both models is that they can exist in particular domains of the parameter space [11,16]. However, the energy band structure due to the periodic potential imposes specific conditions for the existence of multi-D solitons and changes the way by which solitons decay when the border of the existence region is crossed. Specifically, multi-D solitons in a low-D periodic potential can undergo a delocalizing transition into extended Bloch states (in the direction of the OL), similarly to solitons in a full-dimensional periodic potential [16]. Therefore, the norm (number of atoms) of multi-D solitons in a periodic potential is bound not only from above by the onset of collapse, but also from below due to the phenomenon of delocalizing transition. Note that the norm of solitons in axially symmetric 3D GPE with attractive nonlinearity is bound only from above [10–12].

In optics, solitons supported by the low-D periodic structure may find new applications. Indeed, in an optical medium with the full-dimensional periodic potential, transfer of a trapped beam from one position to another is difficult, as the necessary external push strongly disturbs the beam [9]. In the low-D potential, the beam can slide along the free direction, making the transfer easy. In BEC's trapped in a low-D OL, matter-wave solitons can be driven in the free direction by a weak laser beam.

The rest of the paper is organized as follows. In Sec. II, we formulate the 2D and 3D versions of the model and develop the variational approximation (VA) for the solitons based on Gaussian *Ansätze*. In the same section, we compare predictions of the VA with results of direct numerical simulations of the GPE in real time. In particular, a finite interval of values of the norm (number of atoms, in the case of the BEC) in which 2D solitons exist is identified.

Systematic presentation of numerical results is given in Sec. III. In that section, stationary solitons, which may take both single- and multiple-peaked shapes, are found by means of the integration of the GPE in imaginary time. Stable localized pulses are also found in the repulsive model. Then, collisions between the mobile solitons are investigated.

In the attractive model, collisions between single-peaked solitons are studied both inside one channel and in adjacent channels. For identical in-phase solitons, the most interesting outcomes of the collision in one and adjacent channels are, respectively, formation of a collapsing pulse and matter exchange between colliding solitons. Two π-out-of-phase identical solitons in one channel, additionally confined by the external parabolic trap, perform periodic oscillations, each time bouncing elastically from each other. The slow collision between identical in-phase multiple-peaked solitons, whose central peaks are separated by an intermediate channel, results in the formation of one single-peaked soliton in the middle channel, $\simeq 1/3$ of the initial norm being lost with emitted radiation. In the repulsive model with the parabolic trap, two pulses in the same channel behave as true solitons, performing recurrent elastic collisions; at the stage of strong overlap between them, a sharp matter-wave interference pattern emerges periodically.

The paper is concluded by Sec. IV.

II. MODEL AND VARIATIONAL ANALYSIS

The normalized 2D self-focusing NLSE with a Q1D periodic potential of the strength ε is

$$iu_t + \nabla^2 u + [\varepsilon \cos(2x) + \chi|u|^2]u = 0, \tag{1}$$

where $\nabla^2 = \partial_{xx} + \partial_{yy}$, and $\chi = \pm 1$ corresponds to the self-attraction and repulsion. In BEC's, t is time, while in optics it is the propagation distance. For BEC's or spatial optical solitons, x and y are transverse coordinates; for spatiotemporal optical solitons in a 2D waveguide with anomalous chromatic dispersion, y is the "local time." In the context of BEC's, Eq. (1) is usually called the Gross-Pitaevskii equation. The 3D version of Eq. (1) is

$$iu_t + \Delta u + \{\varepsilon[\cos(2x) + \cos(2y)] + \chi|u|^2\}u = 0, \tag{2}$$

where $\nabla^2 = \partial_{xx} + \partial_{yy} + \partial_{zz}$. Equations (1) and (2) conserve the norm $N = \int |u(\mathbf{r})|^2 d\mathbf{r}$ (which is the number of atoms in the BEC or total power and energy of the spatial and spatiotemporal optical solitons), the Hamiltonian, and the momentum along the free direction. The equations are normalized so that the period of the potential is π, the control parameters being ε and N.

Stationary solutions to Eq. (1) are $u(x,y,t) = U(x,y)\exp(-i\mu t)$, with a chemical potential μ (alias the propagation constant, in optics), which leads to an equation

$$\mu U + U_{xx} + U_{yy} + [\varepsilon \cos(2x) + \chi U^2]U = 0 \tag{3}$$

and similar in the 3D case. Multiplication of Eq. (3) by $U(x,y)$ and integration in the plane (x,y) yield the expression

$$\mu = \frac{1}{N}\int_{-\infty}^{\infty} [|\nabla u|^2 - \varepsilon \cos(2x)|u|^2 - \chi|u|^4] dxdy. \tag{4}$$

In the case of very large ε (tens of recoil energy), the Q1D potential valleys become isolated, splitting the 2D BEC into a set of parallel nearly 1D cigar-shaped condensates.

The first step in the analysis is to apply the VA to Eq. (3). To this purpose, we adopt the *Ansätze*

$$U_{2D} = A \exp\left[-\frac{1}{2}(ax^2 + by^2)\right], \tag{5}$$

$$U_{3D} = A \exp\left[-\frac{1}{2}(a(x^2 + y^2) + bz^2)\right], \tag{6}$$

in the 2D and 3D cases, respectively, with the norms

$$N_{2D} = \pi A^2/\sqrt{ab}, \quad N_{3D} = \pi^{3/2}A^2/(a\sqrt{b}). \tag{7}$$

The effective Lagrangians corresponding to Eq. (3) and these *Ansätze* are

$$L_{2D} = N_{2D}\left[a + b - 2\mu - 2\varepsilon e^{-1/a} - \frac{\chi}{2\pi}\sqrt{ab}N_{2D}\right],$$

$$L_{3D} = N_{3D}\left[2a + b - 2\mu - 4\varepsilon e^{-1/a} - \frac{\chi}{(2\pi)^{3/2}}a\sqrt{b}N_{3D}\right].$$

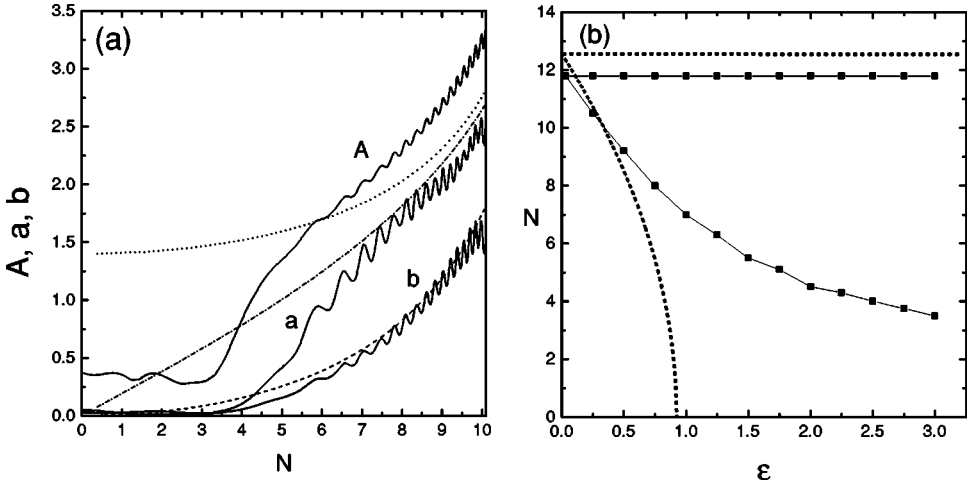

FIG. 1. (a) Parameters of stable 2D solitons in the quasi-1D potential with $\varepsilon=2$, as found from numerical simulations of the Gross-Pitaevskii equation (1) as described in the text (solid lines) and as predicted by the VA for amplitude A (dotted line) and inverse squared widths a and b (dot-dashed and dashed lines, respectively). (b) The numerically found (connected squares) and VA-predicted (dashed lines) existence limits for stable 2D solitons in the quasi-1D potential.

Following a known procedure [13], we derive the variational equations from these Lagrangians: in the 2D case, they are

$$N\chi = (4\pi/a)\sqrt{a^2 - 2\varepsilon\aleph}, \quad \aleph \equiv e^{-1/a}, \tag{8}$$

$$\mu = -a - \varepsilon\aleph(1 - 3/a) \tag{9}$$

(the subscript 2D is suppressed here), and in the 3D case,

$$N\chi = 2(2\pi/a)^{3/2}\sqrt{a^2 - 2\varepsilon\aleph}, \tag{10}$$

$$\mu = -a/2 - \varepsilon\aleph(2 - 3/a). \tag{11}$$

In either case, the remaining variational equation is

$$b = a - 2\varepsilon\aleph/a. \tag{12}$$

Evidently, solutions to Eqs. (8) and (10) are only possible if $\chi>0$ (self-attraction). This does not mean that solitons may not exist with $\chi<0$, but rather that the *Ansätze* (5) and (6) are irrelevant in the case of repulsion.

Figure 1(a) shows the soliton parameters A, a, and b for the 2D soliton, which were found, as functions of the norm, from the variational equations (7), (8), and (12) and from direct numerical simulations of the GPE (1), starting with the initial condition taken as the VA-predicted soliton with a given norm N. Parameters A, a, and b of the established soliton produced by the simulations were measured by fitting it to the wave form (5). The agreement between the VA and direct numerical results is reasonable for $N\gtrsim 5$. In the simulations, the VA-predicted solitons with the norm below this value (in the OL with the strength $\varepsilon=2.0$) spread out into delocalized Bloch states [16], which is manifested as a rapid decrease of the amplitude and inverse width.

Note that, in the direction of the periodic potential (x), the energy spectrum of the linearized GPE (1) exhibits a usual band structure. In this sense, the localized nonlinear state is expected to be a gap soliton, which is the main difference from solitons in axially symmetric 3D GPE considered in [10,11]. To check this conjecture, values of the chemical potential μ of the stable solitons produced by the direct simulations were evaluated by means of Eq. (4). As a result, it was concluded that μ indeed belongs to the corresponding band gap (below the first band) of the underlying linear problem. When the parameters N and ε fall below some critical values, the value of μ predicted by the VA through Eq. (9) moves into the allowed band for the linear Bloch states, which naturally explains the sudden delocalization of the initial wave form in the simulations.

Solving the 2D variational equation (8) for a, one can easily find that the solutions exist in the interval

$$N_{\min} \equiv 4\pi\sqrt{1 - \varepsilon/\varepsilon_{\rm cr}} < N < N_{\max} \equiv 4\pi \tag{13}$$

[see Fig. 1(b)], if $\varepsilon<\varepsilon_{\rm cr}\equiv e^2/8\approx 0.924$, and the interval $0<N<4\pi$, if $\varepsilon>\varepsilon_{\rm cr}$. Unlike this, the solutions for the 3D variational equation (10) can be found for any N with any value of ε. The actual lower limit of the existence region for the 2D solitons in the Q1D periodic potential, determined from direct simulations of the 2D GPE (1) (at the existence border, the initial pulse spreads out into a quasilinear delocalized Bloch state), is shown in Fig. 1(b) by squares. The corresponding upper limit of the existence region is determined numerically by slowly increasing the norm [via the coefficient χ in Eq. (1)] of an established soliton. When the norm exceeds the value $N_{\max}^{(\rm num)}\simeq 11.7$ [which is the actual norm of the *Townes soliton* [8] and is to be compared to the VA prediction, $N_{\max}\equiv 4\pi$ in Eq. (13)], solitons start to radiate matter waves (which are absorbed on the domain boundaries in the numerical algorithm used). We stress that the soliton with the norm somewhat exceeding the value $N_{\max}^{(\rm num)}$ does not commence collapsing, as would be the case with the 2D NLSE in the free space, but rather relaxes back to $N=N_{\max}^{(\rm num)}$, shedding off the excess norm. Therefore, the Q1D potential plays a stabilizing role in this case too, preventing the onset of the collapse.

The above presentation of the VA soliton solutions did not include the dependences $\mu(N)$. Although μ is not a directly observable quantity, these dependences are important too, as, pursuant to the *Vakhitov-Kolokolov* (VK) criterion [14], solution families which meet the condition $d\mu/dN<0$ may be stable, while ones with $d\mu/dN>0$ should be unstable. Therefore, these dependences, obtained, in the 2D and 3D cases, by means of Eqs. (9) and (11), respectively, are displayed in Fig. 2. As is seen, parts of the families definitely

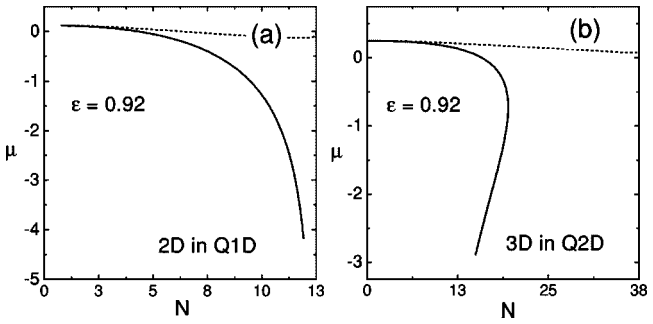

FIG. 2. The $\mu(N)$ dependences for the 2D (a) and 3D (b) solitons in the quasi-1D and quasi-2D potentials, respectively, which make it possible to predict the solitons' stability on the basis of the Vakhitov-Kolokolov criterion. This criterion sets $d\mu/dN<0$ as a necessary stability condition. In each panel, the solid and dashed curves show two different branches of the solution family.

have a negative slope $d\mu/dN$; hence, they may correspond to stable soliton solutions.

III. NUMERICAL RESULTS

A. Stationary solitons

For the purpose of the comparison with predictions of the VA, in the previous section soliton solutions were generated numerically by means of the direct simulations of Eq. (1). In this case, the VA-predicted wave form inserted as an initial condition to Eq. (1) transforms into a stable soliton, shedding a small amount of radiation which is absorbed on the domain boundaries. A more direct way to generate numerically exact stationary soliton solutions is based on the solution of the GPE in imaginary time [15]. We employed this method, also starting with the VA-predicted wave forms, to speed up the convergence. The propagation in imaginary time was run until the chemical potential of the stationary state, Eq. (4), would converge to the accuracy of 10^{-6}. Then, stability of the thus found soliton was verified by direct simulations in real time.

For the stability test, small initial perturbations were explicitly added to the soliton, so that it was taken as $u_0(x,y)=U(x,y)[1+\sigma u_p(x,y)]$, where $U(x,y)$ is the numerically found stationary soliton, σ is a small amplitude, and random functions $u_p(x,y)$ account for the form of the small perturbations. As a result, it was found that the 2D solitons are stable in their *entire existence region*, which was shown in Fig. 1(b). In the 3D model, the solitons were found and tested for the stability in a similar way.

Typical examples of the stable 2D and 3D solitons in the attractive model ($\chi=+1$) are displayed in Figs. 3 and 4. Note that the 3D solitons are nearly isotropic in the (x,y) plane and elongated in the free direction z. As well as in the model with the full (rather than low-dimensional) potential [7], the solitons can be classified into *single-* and *multiple-peaked* ones, with the matter trapped, respectively, in a single potential valley or several adjacent ones. The solitons tend to become multiply peaked for the smaller norm and/or weaker OL. Examples of both types in the 2D model are shown in

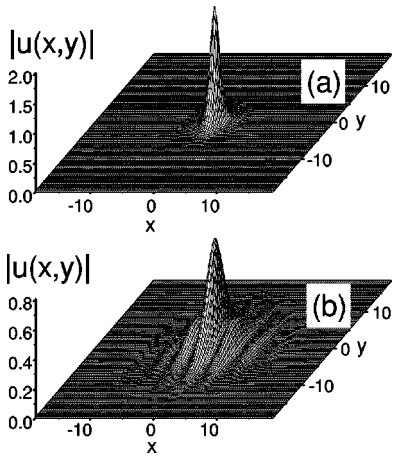

FIG. 3. Examples of single- and multiple-peaked stable 2D solitons supported by the quasi-1D potential (with $\varepsilon=2$) in the model with attraction. The norm and chemical potential of the soliton are $N=2.5\pi, \mu=-1.541$ (a) and $N=1.5\pi, \mu=-0.552$ (b).

Fig. 3. While Fig. 4 displays only an example of the single-peaked 3D solitons, their multiple-peaked counterparts can be easily found too.

The 3D model can also be considered with a Q1D potential. In this case, the VA predicts that *all* the solitons are VK unstable. Accordingly, simulations never produced stable solitons in this case. This feature can be explained by the fact that, in the free 2D subspace orthogonal to the OL, the soliton is essentially tantamount to the above-mentioned unstable Townes soliton. Another relevant remark is that stable solitons with intrinsic vorticity are also possible in the 2D GPE with the fully dimensional 2D lattice [7]. Vortices were found in the present 2D model with the Q1D potential too, but they are always unstable.

In the case of the self-repulsion, $\chi=-1$, the low-D lattice potential cannot support a completely localized pulse. However, adding the parabolic trap readily gives rise to stable configurations which are, essentially, solitons across the lattice and Thomas-Fermi-like states along the free direction

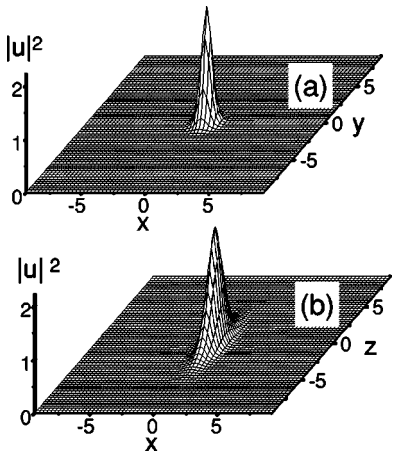

FIG. 4. A stable single-peaked 3D soliton, supported by the quasi-2D potential, with $N=2\pi$ and $\varepsilon=5.0$, in the model with attraction, is shown through its $z=0$ (a) and $y=0$ (b) cross sections.

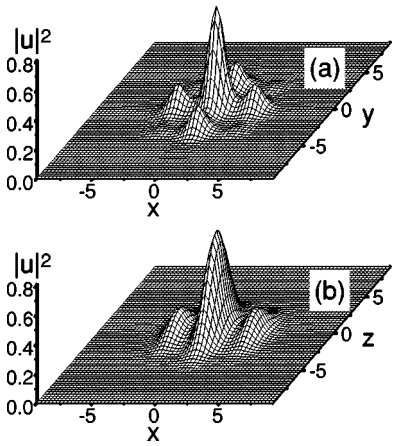

FIG. 5. A stable 3D localized state in the model with repulsion, including a combination of the periodic quasi-2D potential and weak parabolic trap, $V(x,y,z)=2[\cos(2x)+\cos(2y)]-0.01(x^2+y^2)-0.1z^2$. The solution is shown through its $z=0$ (a) and $y=0$ (b) cross sections. The norm of the localized state is $N=4\pi$.

(below, it will be demonstrated that a *pair* of moving and periodically colliding localized pulses, which behave virtually like true solitons, can be created in the 2D and 3D repulsive models with the low-D potential). An example of a stable 3D localized state of this type in the repulsive model is given in Fig. 5.

These configurations assume a multiple-peaked or single-peaked shape under the action of a weaker or stronger OL potential, respectively, which is *opposite* to what was reported above for $\chi>0$; cf. Fig. 3. An explanation to this difference is that, in the case of the self-repulsion and $\varepsilon=0$, no solitons exist at all (even unstable ones, like the above-mentioned Townes soliton).

B. Collision of solitons in the attractive model

Multidimensional solitons in periodic potentials found so far in various settings [2,4,5,7,16] are pinned by the lattice, while it is well known that the most interesting dynamical properties of ordinary solitons are related to their collisions. Accordingly, the mobility in the free direction combined with the possibility off-center collisions in adjasent channels of the periodic potential is the most essential difference of the present multi-D solitons from those predicted in other models.

We have studied the motion of the solitons in the presence of the parabolic trap. If the 2D or 3D soliton is displaced from the central position, it performs harmonic oscillations along the free direction, completely preserving its integrity. When two identical solitons are placed symmetrically off center in the same channel (potential valley), their interaction crucially depends on the phase difference between them. In simulations, 2D and 3D in-phase solitons (the ones with the zero phase difference) which collide head-on with velocities $\pm v$ (which are actually acquired due to the acceleration in the parabolic potential) merge into a single intermediate pulse, provided that the velocity v is below a threshold value v_0. For instance, $v_0=8.5$ for the 2D solitons in the case of $\varepsilon=2.0$ (in this case, the norm of the 2D soliton *per se* is $N=2.5\pi$); an estimate for the threshold velocity in a typical BEC setting yields a really large value in physical units, $v_0\sim 10$ cm/s. In the 2D case, the norm of the intermediate pulse always *exceeds* the critical value $N_{\max}$ [see Eq. (13)] ; therefore, it quickly collapses, and the same happens in the 3D case. These are manifestation of the inelasticity of collisions of multi-D solitons. The inelasticity of collisions of 3D solitons in axially symmetric 3D GPE expressed as an exchange of matter between interacting solitons and their merging was studied in Refs. [10,11]. Particularly, merging of neighboring pulses in a soliton train [10,11] was considered in the context of "missing solitons" in the experiment [17].

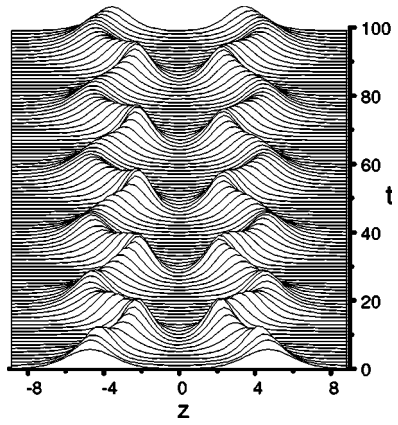

FIG. 6. Oscillations of two π-out-of-phase 3D solitons in the combined OL and weak-harmonic-trap potential, $V(x,y,z)=5[\cos(2x)+\cos(2y)]+0.005z^2$. Parameters are the same as in Fig. 4.

In the case of $v>v_0$, the in-phase solitons colliding in one channel pass through each other, which is explained by the fact that, for solitons with the normalized size ~ 1 [see Figs.

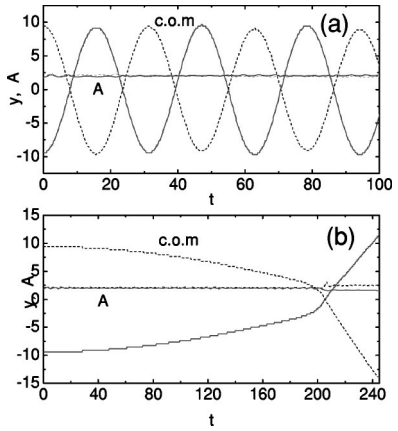

FIG. 7. Center-of-mass trajectories (c.o.m) and amplitudes (A) of two identical 2D solitons colliding in adjasent tracks of the quasi-1D potential ($\varepsilon=2$). (a) When the relative velocity at collision is large (induced by a potential $V_{\text{accel}}=0.001y^2$ in the free direction) solitons collide almost elastically with no exchange of matter and preserving their amplitude. (b) As opposed, slow collisions ($V_{\text{accel}}=0.00001y^2$) are inelastic with strong exchange of metter resulting in different amplitudes and velocities of solitons after the collision. The parameters of solitons are the same as in Fig. 3(a).

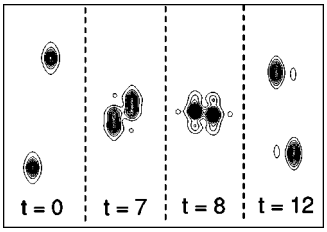

FIG. 8. Contour plots of two identical single-peak 2D solitons colliding at velocities $v=\pm 0.3$ ($\simeq 3$ mm/s, in the typical physical case) in adjacent channels of the quasi-1D potential, with the strength $\varepsilon=1.5$. The norm of each soliton is $N=2\pi$.

3(a) and 4], the collision time $\sim 1/v$ becomes smaller than the collapse time, which may be estimated as being $\sim 1/N$. Identical π-out-of-phase solitons always bounce back if they collide in one channel; as a result, two such solitons in the trap perform indefinitely many stable oscillations with periodic elastic collisions, as shown in Fig. 6.

In the low-D potential, collisions are also possible between solitons moving in *adjacent channels*. If the relative velocity is sufficiently large, such collisions (including recurrent collisions in the presence of a weak parabolic trap) are always completely elastic; see an example in Fig. 7(a). If the relative velocity is small, notable exchange of matter between solitons takes place, and the two solitons emerge with different amplitudes and velocities after the collision [Fig. 7(b)]. At some parameters a collision may result in capturing a "satellite" in the other channel by each soliton, which is shown in detail in Fig. 8. The matter exchange between solitons colliding in adjacent channels is enhanced not only with the decrease of the relative velocity, but also with the decrease of ε, as, naturally, the coupling between the adjacent channels becomes stronger in this case.

Another interesting case is the collision between *multiple-peaked* solitons, such those shown above in Fig. 3(b), whose central peaks are set in two channels separated by an intermediate one. Obviously, only satellite peaks experience the head-on interaction in this configuration. This experiment may test the intrinsic cohesion of the multiple-peaked solitons. To set the solitons in motion, they were, as above, initially placed at some distance from each other in the presence of the external "accelerator"—i.e., a parabolic potential of the form $V_{\rm accel}=\gamma y^2$ (recall that y is the free direction of the Q1D periodic potential). The corresponding configuration is shown in Fig. 9. In some cases, the accelerator with a relatively large strength γ (for instance, $\gamma=0.1$) was switched on for a finite time Δt (typically, $\Delta t \simeq 1$), and then the motion of the solitons in the y direction was completely free.

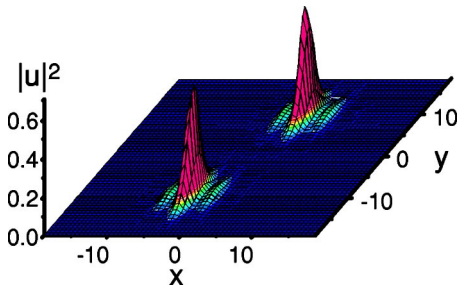

FIG. 9. (Color online) The initial set of two multiple-peaked 2D solitons, each with the norm $N=1.5\pi$, designed for the sideline collision between them, after they were accelerated by the parabolic potential.

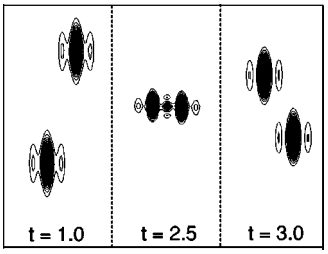

FIG. 10. Contour density plots showing a typical example of the collision, with a moderately large velocity, between two multiple-peaked 2D solitons whose central peaks are separated by an intermediate channel, so that only satellite peaks experience the head-on interaction. In this case, $\varepsilon=2$, the initial norm of each soliton is $N=1.5\pi$. The solitons are accelerated by the external potential γy^2 with $\gamma=0.1$, which acted temporarily, during the time $\Delta t=1$, and was then switched off.

In the case of a moderately large relative velocity, the collision of this type results in small changes of the solitons' shapes due to a weak matter exchange between them. A typical example of this sort is shown, by means of contour density plots, in Fig. 10. The small perturbation of the solitons' shapes after the collision confirms that the multiple-peaked solitons are robust intrinsically coherent objects. The same conclusion follows from simulations of similar collisions between multiple-peaked 3D solitons (not shown here).

With a smaller relative velocity of the solitons, the collision of the same type between the in-phase multiple-peaked solitons produces a drastically different result, as shown in Fig. 11 (the result is altogether different too from what was

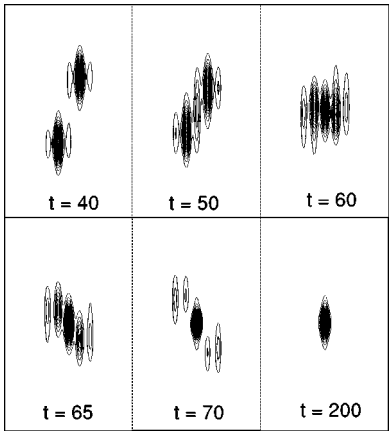

FIG. 11. A typical example of the slow collision between two identical in-phase multiple-peaked 2D solitons, with their central peaks originally separated by the intermediate channel. Eventually, one *single-peaked* soliton appears, trapped in the middle channel, a part of the initial norm being lost with radiation. Parameters are the same as in Fig. 10 except that the collision velocity is smaller (the accelerating potential, γy^2 with $\gamma=0.001$, acted during the time $\Delta t=10$). The norm of the resulting single-peaked soliton is $N \approx 2\pi$, which is 2/3 of the total initial norm.

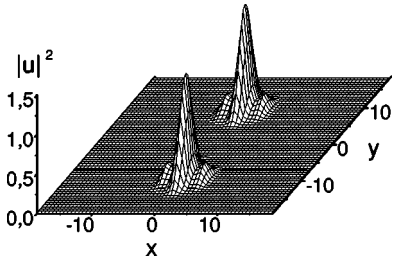

FIG. 12. The initial set of two 2D localized states in the repulsive BEC, created at some distance from each other by means of a potential barrier separating them in the direction y. The norm of each soliton is $N=4\pi$.

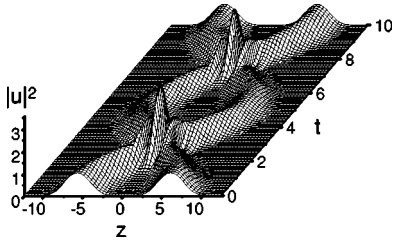

FIG. 14. Recurrent collisions of two 3D solitons in the repulsive model, shown through the $y=0$ cross section. Parameters are the same as in Fig. 5.

observed in collisions of two in-phase single-peaked solitons placed in adjacent channels; see Fig. 8). In this case, a large share of matter from the central peaks of both solitons can tunnel, during the collision, into the middle channel, where the satellite peaks experience the head-on collision. Eventually, the two multiple-peaked solitons end up forming one *stable* (undercritical, in the 2D case) *single-peaked soliton*, whose norm is smaller than the initial total norm of the configuration (for instance, it is $2/3$ of the initial norm in the case shown in Fig. 11). The loss of the norm is due to emission of linear waves in the course of the collision; this radiation is absorbed at edges of the integration domain.

C. Collision of solitons in the repulsive model

Recent experiments with repulsive BEC's loaded in moving OL's offer evidence in favor of the existence of bright matter-wave solitons of the gap type [18]. Modulational instability and a negative effective mass, which are considered to be at the origin of the bright-soliton formation in repulsive BEC's with the periodic potential, have been observed too [19,20] (the negative effective mass was observed indirectly, through an optically induced lensing effect). These developments suggest the feasibility of the experimental observation of gap-type solitons in repulsive BEC's in the 2D and 3D cases too, which justifies theoretical analysis of their dynamical properties.

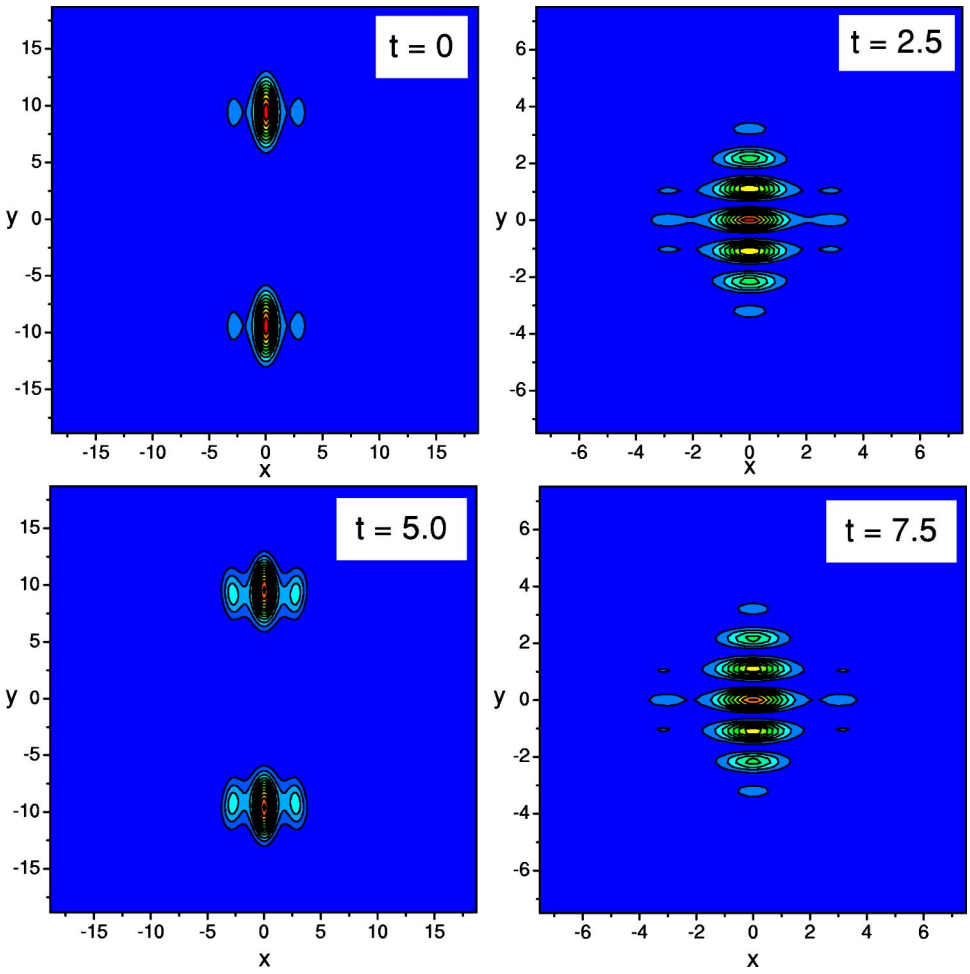

FIG. 13. (Color online) Recurrent head-on collisions (in one channel of the quasi-1D periodic potential) of two 2D localized pulses in the repulsive BEC. The pulses periodically pass through each other, with a period $T\simeq 10$. At the moments of the full overlap—viz., $t=2.5$, $t=7.5$, and so on (the same picture is observed at $t=12.5$)—i.e., each half-period, sharp interference fringes are evident (note that the right panels are enlarged).

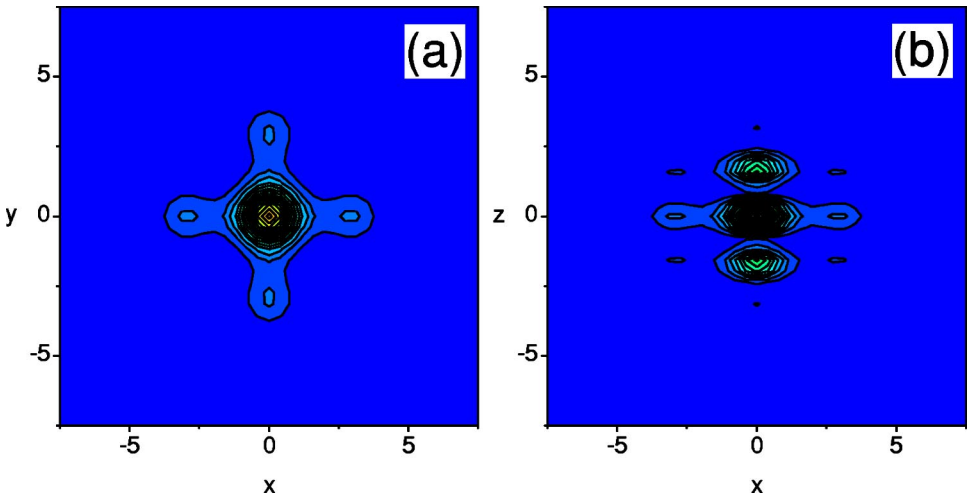

FIG. 15. (Color online) Contour plots illustrating the periodic collisions of two 3D solitons in the repulsive model, at the moment of the full overlap between them ($t=2.5$). The panels (a) and (b) correspond to the cross sections $z=0$ and $y=0$, respectively.

As was pointed out above, the creation of stable localized states in the repulsive case in a low-D periodic potential requires confinement in the free direction. An example of a 3D soliton created in the center of the combined Q2D OL and parabolic-trap potentials was displayed in Fig. 5. The creation of *two* such localized states at some distance from each other along the free direction is possible by applying an additional potential barrier (for instance, in the form of a Gaussian) separating them. Then, a collision between the pulses can be induced by suddenly removing the barrier. A similar technique was employed in the interference experiments with two BEC's released from a double-well potential [21]. As a result (see Figs. 12 and 13 which illustrate the 2D case), the pulses, which actually behave like true solitons in this situation, emerge *unscathed* after periodic collisions, passing through each other in an elastic fashion. A characteristic signature of the collision is a pattern of matter-wave interference fringes, periodically appearing when the solitons overlap. In fact, a similar effect can also be observed in head-on collisions between fast solitons in the attractive model (otherwise, it is eclipsed by the ensuing collapse).

Collisions between solitons inside one channel were investigated in the 3D repulsive model too. As well as in the 2D case, initial pulses were prepared by means of a separating barrier, which was then suddenly lifted. As is seen from Figs. 14 and 15 pertaining to the 3D model, in this case the collisions also turn out to be periodic and completely elastic, and a sharp interference pattern is again observed at the overlap stage.

IV. CONCLUSION

We have demonstrated that periodic potentials whose dimension is smaller by 1 than the full spatial dimension can support stable single- and multiple-peaked solitons in 2D and 3D self-focusing media (while the quasi-1D potential cannot stabilize 3D solitons), which suggest new settings for experimental search of multidimensional (multi-D) solitons in photonic crystals and Bose-Einstein condensates. The 2D solitons exist in a finite interval of the values of the norm, which is predicted by the variational approximation and is borne out by direct simulations. In the case of self-repulsion, stable localized states are found too, provided that the model includes the parabolic trap. Evolution of their structure is opposite to that in the case of the self-attraction: with the increase of the strength of the low-D periodic potential, a single-peaked state is changed by a multiple-peaked one.

These solitons are the first example of mobile multi-D pulses predicted in BEC's, which suggests to study collisions between them (in the 2D setting, the collisions may also be realized in photonic crystals). The head-on collisions of in-phase solitons lead to their fusion and collapse (unless the relative velocity is very large), while out-of-phase solitons collide elastically indefinitely many times (if they are confined by the external parabolic trap). The collision between multiple-peaked solitons whose central peaks are separated by an intermediate channel may lead to the formation of one single-peaked soliton in the middle channel, the excess matter being shed off. Thus, a fundamental feature dominating various types of the collisions in the attractive model is the exchange of matter between the solitons. The inelasticity of multi-D soliton collisions, expressed as a matter exchange between solitons, appears to be similar as in the model with axially symmetric 3D GPE [10,11].

In the repulsive model, stable localized states of the mixed solitonic–Thomas-Fermi type are supported by the low-D potential combined with a parabolic trap. Two such pulses can be created in one channel by means of an extra transverse potential barrier. After lifting the barrier, the pulses perform recurrent elastic collisions (i.e., they behave like true solitons), with a sharp interference pattern emerging when they periodically overlap.

ACKNOWLEDGMENTS

We appreciate valuable discussions with Y. S. Kivshar. B.B. thanks the Department of Physics at the University of Salerno (Italy) for a research grant. B. M. appreciates the hospitality of the same department and partial financial support through Grant No. 8006/03 from the Israel Science Foundation. M.S. acknowledges partial financial support from the MIUR, through interuniversity Project No. PRIN-2003, and from European LOCNET Grant No. HPRN-CT-1999-00163.

[1] P. Xie, Z.-Q. Zhang, and X. Zhang, Phys. Rev. E **67**, 026607 (2003); A. Ferrando, M. Zacares, P. F. de Cordoba, D. Binosi, and J. A. Monsoriu, Opt. Express **11**, 452 (2003).

[2] J. Fleischer, M. Segev, N. Efremidis, and D. N. Christodoulides, Nature (London) **422**, 147 (2003); J. W. Fleischer, G. Bartal, O. Cohen, O. Manela, M. Segev, J. Hudock, and D. N. Christodoulides, Phys. Rev. Lett. **92**, 123904 (2004); D. Neshev, T. J. Alexander, E. A. Ostrovskaya, Y. S. Kivshar, H. Martin, I. Makasyuk, and Z. Chen, *ibid.* **92**, 123903 (2004); Z. Chen, H. Martin, E. D. Eugenieva, J. Xu, and A. Bezryadina, *ibid.* **92**, 143902 (2004).

[3] M. Greiner, O. Mandel, T. Esslinger, T. W. Hansch, and I. Bloch, Nature (London) **415**, 39 (2002); M. Greiner, O. Mandel, T. W. Hansch, and I. Bloch, *ibid.* **419**, 51 (2002); I. Bloch, M. Greiner, O. Mandel, and T. W. Hansch, Philos. Trans. R. Soc. London, Ser. A **361**, 1409 (2003).

[4] B. B. Baizakov, V. V. Konotop, and M. Salerno, J. Phys. B **35**, 5105 (2002).

[5] E. A. Ostrovskaya and Y. S. Kivshar, Phys. Rev. Lett. **90**, 160407 (2003); N. K. Efremidis, J. Hudock, D. N. Christodoulides, J. W. Fleischer, O. Cohen, and M. Segev, Phys. Rev. Lett. **91**, 213906 (2003).

[6] H. Sakaguchi and B. A. Malomed, J. Phys. B **37**, 1443 (2004).

[7] B. B. Baizakov, B. A. Malomed, and M. Salerno, Europhys. Lett. **63**, 642 (2003); J. Yang and Z. Musslimani, Opt. Lett. **23**, 2094 (2003).

[8] L. Bergé, Phys. Rep. **303**, 260 (1998).

[9] B. A. Malomed, Z. H. Wang, P. L. Chu, and G. D. Peng, J. Opt. Soc. Am. B **16**, 1197 (1999).

[10] L. Salasnich, A. Parola, and L. Reatto, Phys. Rev. Lett. **91**, 080405 (2003).

[11] S. K. Adhikari, New J. Phys. **5**, 137 (2003).

[12] L. Salasnich, A. Parola, and L. Reatto, Phys. Rev. A **66**, 043603 (2002).

[13] B. A. Malomed, P. Drummond, H. He, A. Berntson, D. Anderson, and M. Lisak, Phys. Rev. E **56**, 4725 (1997).

[14] M. G. Vakhitov and A. A. Kolokolov, Radiophys. Quantum Electron. **16**, 783 (1973).

[15] M. L. Chiofalo, S. Succi, and P. Tosi, Phys. Rev. E **62**, 7438 (2000).

[16] B. B. Baizakov and M. Salerno, Phys. Rev. A **69**, 013602 (2004).

[17] K. E. Strecker, G. B. Partridge, A. G. Truscott, and R. G. Hulett, Nature (London) **417**, 150 (2002).

[18] B. Eiermann, Th. Anker, M. Albiez, M. Taglieber, P. Treutlein, K. -P. Marzlin, and M. K. Oberthaler, Phys. Rev. Lett. **92**, 230401 (2004).

[19] M. Cristiani, O. Morsch, N. Malossi, M. Jona-Lasinio, M. Anderlini, E. Courtade, and E. Arimondo, Opt. Express **12**, 4 (2004).

[20] L. Fallani, F. S. Cataliotti, J. Catani, C. Fort, M. Modugno, M. Zawada, and M. Inguscio, Phys. Rev. Lett. **91**, 240405 (2003).

[21] M. R. Andrews, C. G. Townsend, H. -J. Miesner, D. S. Durfee, D. M. Kurn, and W. Ketterle, Science **275**, 637 (1997).